

# Enhanced photoresponse performance in Ga/Ga<sub>2</sub>O<sub>3</sub> nanocomposite solar-blind ultraviolet photodetectors\*

Shu-Juan Cui(崔书娟)<sup>1,2</sup>, Zeng-Xia Mei(梅增霞)<sup>1,†</sup>, Yao-Nan Hou(侯尧楠)<sup>1</sup>, Quan-Sheng Chen(陈全胜)<sup>1,2</sup>, Hui-Li Liang(梁会力)<sup>1</sup>, Yong-Hui Zhang(张永晖)<sup>1,2</sup>, Wen-Xing Huo(霍文星)<sup>1,2</sup>, and Xiao-Long Du(杜小龙)<sup>1,2,‡</sup>

<sup>1</sup>Beijing National Laboratory for Condensed Matter Physics, Institute of Physics, Chinese Academy of Sciences, Beijing 100190, China

<sup>2</sup>School of Physical Sciences, University of Chinese Academy of Sciences, Beijing 100049, China

(Received 9 February 2018; revised manuscript received 6 March 2018; published online 10 May 2018)

In the present work, we explore the solar-blind ultraviolet (UV) photodetectors (PDs) with enhanced photoresponse, fabricated on Ga/Ga<sub>2</sub>O<sub>3</sub> nanocomposite films. Through pre-burying metal Ga layers and thermally post-annealing the laminated Ga<sub>2</sub>O<sub>3</sub>/Ga/Ga<sub>2</sub>O<sub>3</sub> structures, Ga/Ga<sub>2</sub>O<sub>3</sub> nanocomposite films incorporated with Ga nanospheres are obtained. For the prototype PD, it is found that the photocurrent and photoresponsivity will first increase and then decrease monotonically with the thickness of the pre-buried Ga layer increasing. Each of all PDs shows a spectrum response peak at 260 nm, demonstrating the ability to detect solar-blind UV light. Adjustable photoresponse enhancement factors are achieved by means of the surface plasmon in the nanocomposite films. The PD with a 20 nm thick Ga interlayer exhibits the best solar-blind UV photoresponse characteristics with an extremely low dark current of 8.52 pA at 10-V bias, a very high light-to-dark ratio of  $\sim 8 \times 10^5$ , a large photoresponsivity of 2.85 A/W at 15-V bias, and a maximum enhancement factor of  $\sim 220$ . Our research provides a simple and practical route to high performance solar-blind UV PDs and potential applications in the field of optoelectronics.

**Keywords:** Ga/Ga<sub>2</sub>O<sub>3</sub>, nanocomposite, surface plasmon, solar-blind photodetector

**PACS:** 73.20.Mf, 85.60.Gz, 71.20.Nr, 73.40.Sx

**DOI:** 10.1088/1674-1056/27/6/067301

## 1. Introduction

The term solar-blind ultraviolet (UV) is due to the radiation in this region (220 nm~280 nm) being almost completely absorbed by the ozone layer and thus the background radiation in the atmosphere is close to zero. The black background makes the solar-blind UV photodetector (PD) have low noise and high sensitivity simultaneously. Owing to the huge application prospects in civil and military areas, such as flame monitoring, space communication, biological medicine, and missile guidance, solar-blind UV PDs have been attracting extensive attention.<sup>[1,2]</sup> The high photon energy of solar-blind UV light enables the wide band gap semiconductors to serve as detection materials, including diamond,<sup>[3,4]</sup> AlGa<sub>3</sub>N,<sup>[5,6]</sup> MgZnO,<sup>[7-9]</sup> Ga<sub>2</sub>O<sub>3</sub>, etc.<sup>[10-17]</sup> Compared with other wide band gap materials, Ga<sub>2</sub>O<sub>3</sub> has a direct band gap ( $\sim 4.9$  eV) and a high absorption coefficient ( $> 10^5$  cm<sup>-1</sup> near band edge) in the solar-blind UV spectral region, which avoids the complex band gap engineering problem and makes Ga<sub>2</sub>O<sub>3</sub> a particularly suitable candidate for solar-blind UV photodetection.<sup>[18,19]</sup> To date, bulk,<sup>[11,12]</sup> thin-film,<sup>[13-15]</sup> and nanostructure<sup>[16,17]</sup> Ga<sub>2</sub>O<sub>3</sub> solar-blind UV PDs have been proposed. The bulk and nanostructured Ga<sub>2</sub>O<sub>3</sub> PDs usually exhibit superior sensitivity and photoresponsivity to the solar-blind UV light in contrast to their thin-film counterpart.<sup>[11-17]</sup>

However, the complex synthesis technologies and high cost of the bulk Ga<sub>2</sub>O<sub>3</sub> crystals and the low repeatability of Ga<sub>2</sub>O<sub>3</sub> nanostructures greatly restrict their practical applications. Therefore, thin-film-type PDs are still the main research focus. On the other hand, the reported thin-film-type PDs, which have good photoresponse performances ( $> 1$  A/W), are based on high-quality Ga<sub>2</sub>O<sub>3</sub> single crystalline films.<sup>[14,15]</sup> The growth methods for these high-quality thin-films include molecular beam epitaxy, metal-organic chemical vapor deposition, and pulsed laser deposition, in which usually there are the needs of high-vacuum instruments, high growth temperatures, and complicated processes.<sup>[14,15,20]</sup> The expensive costs and rigorous conditions required by these synthesis techniques significantly restrict the industrial development of large-area films. Obviously, the current Ga<sub>2</sub>O<sub>3</sub> PDs are far away from the industrialization demands, and it is urgently needed to explore a cost-effective and practical method to acquire a unique Ga<sub>2</sub>O<sub>3</sub> material with improved solar-blind photoresponse performance.

Surface plasmon (SP) resonance is the phenomenon of collective electron oscillations on the surfaces of metal nanoparticles driven by incident light.<sup>[21,22]</sup> Under resonance state, the local electromagnetic field around the metal nanoparticles can be greatly enhanced,<sup>[23]</sup> and the scattering cross sec-

\*Project supported by the National Natural Science Foundation of China (Grant Nos. 11674405 and 11675280) and the Fund from the Laboratory of Microfabrication in Institute of Physics, Chinese Academy of Sciences.

†Corresponding author. E-mail: zxmei@iphy.ac.cn

‡Corresponding author. E-mail: xldu@iphy.ac.cn

tion of incident light increases at the same time, which greatly improve the interaction between the light and the material.<sup>[24]</sup> This principle ensures the SP effect, which is widely used in the fields of optoelectronics, such as detectors,<sup>[25–28]</sup> solar cells,<sup>[24]</sup> photocatalysts,<sup>[29]</sup> and Raman detection.<sup>[30]</sup> It is well established that the resonance peak of gallium (Ga) based plasmonic platform is adjustable from the visible to solar-blind UV spectral range.<sup>[31–33]</sup> Recently, we have achieved a Ga/Ga<sub>2</sub>O<sub>3</sub> nanocomposite film through post-annealing the Ga<sub>2</sub>O<sub>3</sub>/Ga/Ga<sub>2</sub>O<sub>3</sub> laminated film, and the corresponding solar-blind PD has remarkably enhanced responsivity due to the SP coupling effect, which will be published elsewhere.<sup>[34]</sup> It should be noted that the thickness of the Ga interlayer plays an important role in the photoresponse properties of Ga/Ga<sub>2</sub>O<sub>3</sub> nanocomposite PDs, and the dependence of the PD performance on this key parameter has to be explored in detail.

Here in this work, we present a series of Ga/Ga<sub>2</sub>O<sub>3</sub> nanocomposite solar-blind PDs with adjustable photoresponse enhancement factors caused by the SP coupling effect. The Ga/Ga<sub>2</sub>O<sub>3</sub> nanocomposite films are obtained by annealing the Ga<sub>2</sub>O<sub>3</sub>/Ga/Ga<sub>2</sub>O<sub>3</sub> triple-layer films in a tube furnace. By changing the thickness of the pre-buried Ga interlayer, the enhancement factor of the responsivity can be increased by about 4.5–220 times. The detector achieves the best solar-blind UV photoresponse performance when the interlayer Ga is 20-nm thick. The low dark current of 8.52 pA at 10-V bias along with the high peak responsivity of 2.85 A/W at 15-V bias indicates that the SP coupled PD is likely to have prospects of practical applications.

## 2. Experimental methods

### 2.1. Fabrication of the nanocomposite films

The Ga/Ga<sub>2</sub>O<sub>3</sub> nanocomposite films were synthesized by post-annealing the laminated Ga<sub>2</sub>O<sub>3</sub>/Ga/Ga<sub>2</sub>O<sub>3</sub> samples. Firstly, 100-nm Ga<sub>2</sub>O<sub>3</sub> film was sputtered on a quartz substrate (500- $\mu$ m thick) in pure argon (Ar) atmosphere at room temperature for about 10 min with a radio frequency of 60 W. Secondly, a metal Ga thin layer was grown on this Ga<sub>2</sub>O<sub>3</sub> film through the thermal evaporation process. Finally, another 100-nm Ga<sub>2</sub>O<sub>3</sub> layer was deposited on the top of the Ga interlayer. The laminated film samples are subsequently annealed at 1050 °C for 30 min. The annealing process was carried out in a GSL-1400X vacuum high-temperature tube furnace. The whole heating and cooling process was implemented in an Ar atmosphere at a flow rate of 200 standard cubic centimeters per minute (sccm), and the pressure was kept at 1 atm (1 atm = 1.01325  $\times$  10<sup>5</sup> Pa). The temperature ramping rates were set to be 10 °C/min. After annealing, the Ga interlayer migrated upwards and formed discrete

metal Ga nanospheres (NSs) embedded in the Ga<sub>2</sub>O<sub>3</sub> matrix, which have been verified through the transmission electron microscopy (TEM) characterizations in our previous work.<sup>[34]</sup> Four Ga/Ga<sub>2</sub>O<sub>3</sub> nanocomposite samples were prepared by annealing the laminated Ga<sub>2</sub>O<sub>3</sub>/Ga/Ga<sub>2</sub>O<sub>3</sub> samples with different Ga layer thickness, denoted as S1 (10-nm Ga), S2 (20-nm Ga), S3 (30-nm Ga), and S4 (40-nm Ga), respectively. A sample with a thickness the same as that of Ga<sub>2</sub>O<sub>3</sub> film and no Ga interlayer annealed under the same conditions was adopted as a control sample, denoted as S0.

### 2.2. Fabrication of the photodetectors

The solar-blind UV PDs were fabricated by conventional UV photolithography and lift-off processes. The Sn-doped indium oxide (ITO, 100 nm) layer was sputtered at room temperature to form the Schottky contacts with the Ga<sub>2</sub>O<sub>3</sub> films. A planar metal-semiconductor-metal (MSM) structure was adopted, with 5  $\mu$ m in width spaced by a 5- $\mu$ m gap, 300  $\mu$ m in length, and 75 pair fingers in total.

### 2.3. Characterization

An atomic force microscope (AFM, Bruker MultiMode 8) was employed to characterize the surface morphology of all the samples. The crystallinity of each of the annealed samples was confirmed by an x-ray diffractor (XRD, Rigaku SmartLab). Transmittance spectra of all samples were measured on a UV-3600 Plus (Shimadzu Corporation) UV-VIS-NIS spectrophotometer.

Due to the ultra-low dark current of the PD, the source-measurement unit in the Keithley 4200 semiconductor characterization system was used to obtain the current–voltage ( $I$ – $V$ ) curve in the dark. In other photoelectric measurements, the Keithley 6487 Picoammeter was used as a power supply. A hand-held lamp with 254-nm UV irradiation was used as a light source for the  $I$ – $V$  curve under illumination and the time-dependent photoresponse. Evaluation of the photoresponse properties of PDs in a range of 200 nm to 600 nm was carried out by using an Omni- $\lambda$  180i grating spectrometer.

For a better illustration of the SP effect on the enhanced solar-blind UV detection capability, the spatial electric field distribution around the Ga NSs and the inter-sphere interaction between two Ga NSs are simulated with the finite-difference time-domain (FDTD) method.

## 3. Results and discussion

Figures 1(a)–1(f) show the AFM images of S0–S4. For S0 sample without Ga interlayer, the surface is relatively smooth, with a root mean square (RMS) roughness value of 2.5 nm [Fig. 1(a)]. For samples S1–S4 with pre-deposited metal Ga layer, dense and uniform crystalline grains are dominated on the surface. The grains tend to grow and to coalesce with the

thickness of Ga layer increasing as shown in Figs. 1(b)–1(e). The specific RMS values for S1, S2, S3, and S4 are 11.5 nm, 22.3 nm, 27.3 nm, and 35.3 nm, respectively. The average diameters of the grains on the surfaces are 150 nm (S1), 185 nm (S2), 245 nm (S3), and 400 nm (S4), respectively. Figure 1(f) shows the detailed three-dimensional surface feature of S2 as an example, where the grains clearly protrude from the surface. Considering the above results, it is supposed that annealing of the pre-buried metal gallium layer contributes to the rough surface. In fact, the surface protrusion in Fig. 1(f)

is composed of the interior discrete metal Ga NSs and the surrounding  $\beta$ -Ga<sub>2</sub>O<sub>3</sub> matrix, which has been confirmed by TEM observations (not shown here). The Ga NSs in S2 is about 10 nm–20 nm in diameter with an adjacent distance of 5 nm–20 nm. Ga NSs with this size and distribution can couple with the energy band of Ga<sub>2</sub>O<sub>3</sub>. Formation of the Ga/Ga<sub>2</sub>O<sub>3</sub> nanocomposite film is caused by the Ga atoms migrating from the interlayer upwards to the surface and their partial oxidation in the thermal annealing process. Therefore, the sample without Ga interlayer (S0) is much smoother.

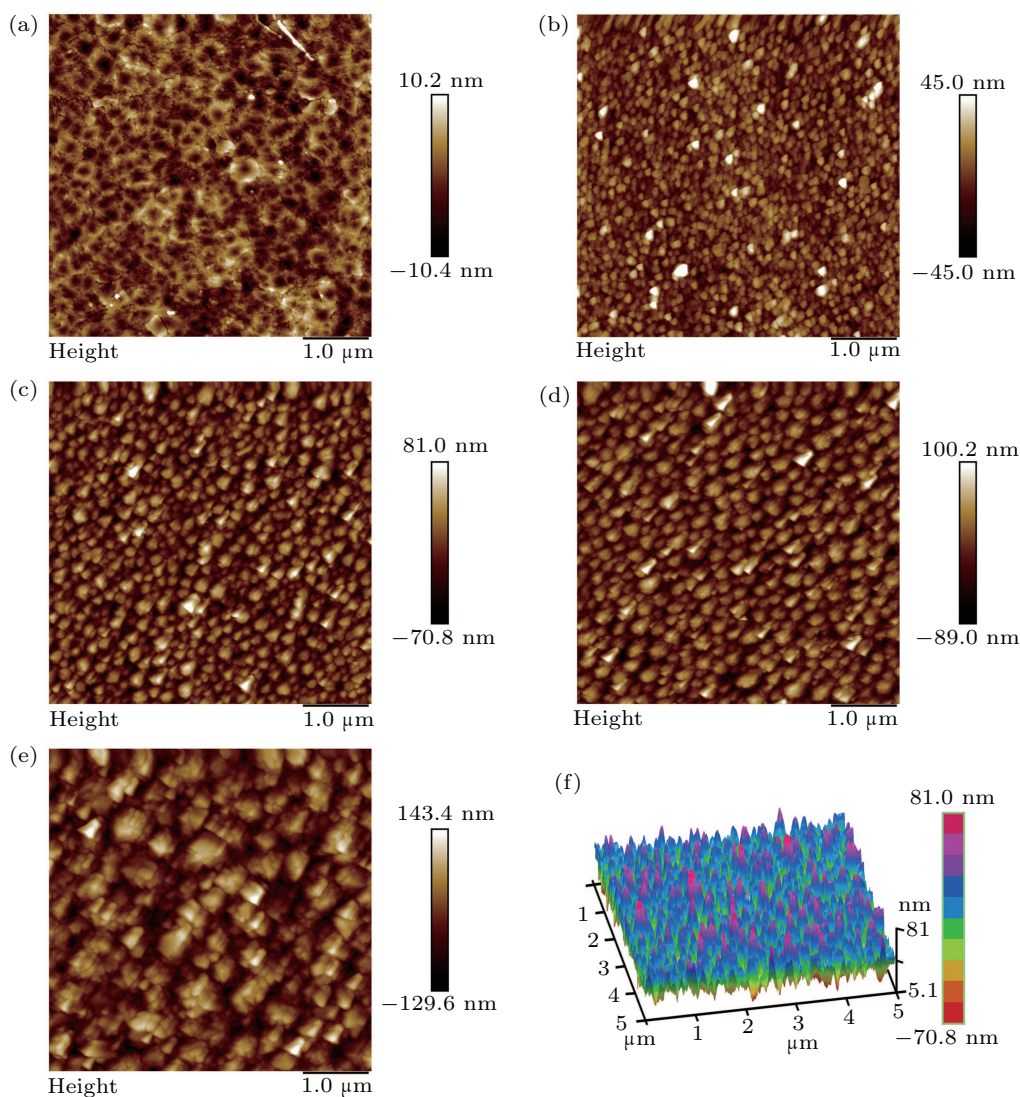


**Fig. 1.** (color online) AFM images of the samples S0–S4: (a) S0 (without Ga layer), (b) S1 (with 10-nm Ga), (c) S2 (with 20-nm Ga), (d) S3 (with 30-nm Ga), (e) S4 (with 40-nm Ga), and (f) three-dimensional feature of S2 (with 20-nm Ga).

To further investigate the crystal structures of all the samples, XRD measurements are carried out. Figure 2(a) reveals that all the diffraction peaks of the bare Ga<sub>2</sub>O<sub>3</sub> sample (S0) can be indexed and belong to the monoclinic structure, in good consistence with those of  $\beta$ -Ga<sub>2</sub>O<sub>3</sub> ( $a = 12.214$  Å,  $b = 3.037$  Å,  $c = 5.798$  Å,  $\beta = 103.8^\circ$ , JCPDS Card No. 87-1901). The four dominant peaks located at  $18.9^\circ$ ,  $30.2^\circ$ ,  $31.8^\circ$ , and  $64.7^\circ$  are assigned to  $(\bar{2}01)$ , (400),  $(\bar{2}02)$ , and  $(\bar{7}12)$

planes respectively, indicating that all the samples are polycrystalline. After incorporating Ga, two remarkable differences occur, in contrast to S0. Firstly, the intensities of  $(\bar{2}01)$  and  $(\bar{2}02)$  planes decrease. Secondly, some new diffraction peaks appear and all of them belong to the planes of monoclinic Ga<sub>2</sub>O<sub>3</sub>. Notably, the intensity of the new peak at  $35.3^\circ$ , coming from  $\beta$ -Ga<sub>2</sub>O<sub>3</sub>(111) plane, increases as the thickness of Ga interlayer increases. The structural evolutions and their



influence on PD performance are not clear and need further investigating.

Transmittance spectra of all the samples are exhibited in Fig. 2(b), where each of all the samples demonstrates transparency in the visible spectrum range with a high transmittance over 75%. The curves of S1–S4 samples with different thickness values of pre-buried Ga layer show various degrees of red shifts compared with that of the bare  $\text{Ga}_2\text{O}_3$  sample (S0). A close view of their absorption edges presents the red shift tendencies of these nanocomposite samples (see the inset of Fig. 2(b)). In addition to the red shift, the transmittance within a region from 300 nm to 500 nm also shows a little degree of gradual decrease with Ga thickness increasing. All the changes in the transmittance spectra are presumably ascribed to the increasing of residual Ga NSs and their sizes in the  $\text{Ga}/\text{Ga}_2\text{O}_3$  nanocomposite films.

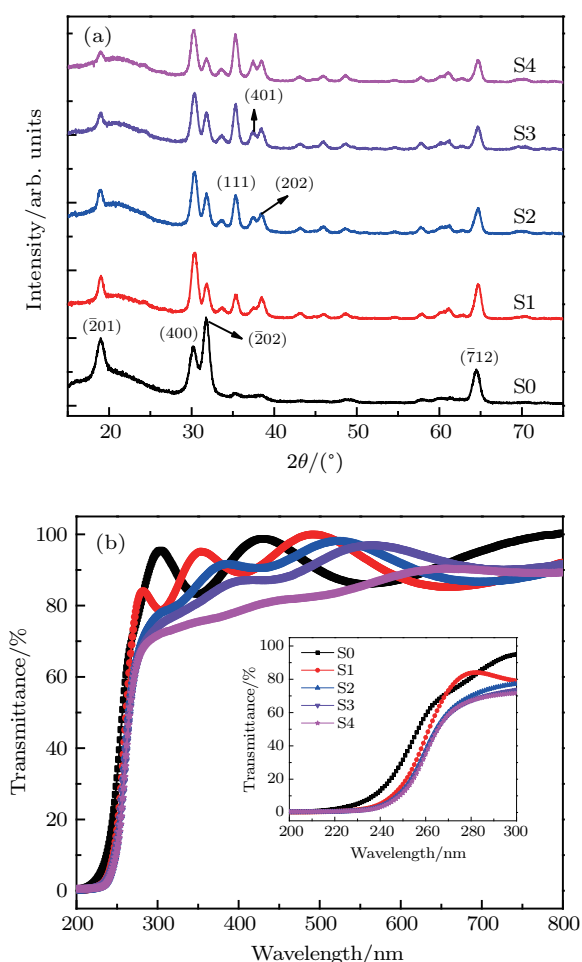


**Fig. 2.** (color online) (a) XRD patterns and (b) optical transmittance spectra of samples S0–S4. Inset shows the magnified curves around the absorption edges.

Prototype solar-blind PDs are fabricated on these samples each with an MSM structure, and their photoresponse performance is shown in Fig. 3. Figure 3(a) presents the  $I$ – $V$  characteristics of the devices in the dark. As the thickness of the Ga interlayer increases, the dark current first in-

creases and then decreases. The S0 illustrates the lowest dark current (only 2.76 pA at 10 V), and S2 has the largest dark current (8.52 pA at 10 V) among all the samples. Actually, the dark currents for all PDs are relatively low compared with previous results.<sup>[14,35–37]</sup> The evolution of photocurrent under the 254-nm UV illumination shown in Fig. 3(b) follows the same trend as the dark current, i.e., S2 exhibits the largest current increment compared with S0. Table 1 shows the photoelectric parameters of all the samples. It can be seen that 10-nm pre-buried Ga can enhance the photocurrent by about two orders of magnitude. Further increasing the thickness of Ga metal layer, the photocurrent can be increased about 300 times for S2. The enhancement ratio of the photocurrent is much larger than that of the dark current whose enhancement is only about 3 times. Therefore, a much higher light-to-dark ratio ( $I_{\text{photo}}/I_{\text{dark}}$ ,  $\sim 8 \times 10^5$  for S2) is achieved when the Ga NSs/ $\text{Ga}_2\text{O}_3$  nanocomposite film is employed as a photo active layer. In order to obtain the information about the response speed and repeatability of the devices, time-dependent deep UV response tests are performed with a UV 254-nm hand-held lamp on and off periodically. As shown in Fig. 3(c), each of all the detectors presents a very stable and repeatable photoresponse behavior. Moreover, there is no obvious change in the rise time nor in the decay time of the device when changing the thickness of the Ga layer. The spectral response characteristics under 15-V bias of the PDs are shown in Fig. 3(d). All the response peaks are located at  $\sim 260$  nm, which is consistent with previous report on the  $\text{Ga}_2\text{O}_3$  detector.<sup>[38]</sup> As summarized in Table 1, the peak responsivity for S0 is only 0.013 A/W. When the samples are embedded with discrete Ga NSs, the responsivities increase dramatically. Especially for sample S2, the responsivity reaches 2.85 A/W, which is an extraordinary promotion compared with the responsivity for S0. The photoresponse enhancement can be adjusted by simply varying the thickness of the metal layer. The big enhancement of the solar-blind UV photoresponse performance results from the SP coupling at the Ga NSs/ $\text{Ga}_2\text{O}_3$  interface. Specifically speaking, the SP facilitates the plasmon-induced resonant energy transfer from metal Ga to  $\text{Ga}_2\text{O}_3$  in the nanocomposite film. In addition, direct hot electron transfer to  $\text{Ga}_2\text{O}_3$  is also probable due to the intimate contact between Ga NSs and  $\text{Ga}_2\text{O}_3$ , which further increases the photocurrent collected. The detailed analysis of the coupling mechanism can be found in our previous report.<sup>[34]</sup> The plasmon peak energy will experience a blueshift with the diameter of the metal particles decreasing.<sup>[31,39–41]</sup> The efficiency of the SP enhancement will reach a maximum when the energy of plasmon is exactly consistent with the band gap of the semiconductor. In these PD devices, the resonance enhancement effect varies with pristine

Ga thickness, the biggest enhancement factor for S2. As the thickness of the middle metal Ga layer increases, the diameter and the density of the Ga NSs gradually increase correspondingly. The sizes and distribution of Ga NSs in S2 provide the best energy coupling between SP and Ga<sub>2</sub>O<sub>3</sub> energy

band. When the NS diameter is too small or too large, the plasmon resonance peak will deviate from the band gap of Ga<sub>2</sub>O<sub>3</sub>, leading to a reduced coupling efficiency. That is why a controllable SP resonance enhancement can be realized by changing the thickness of the Ga layer.

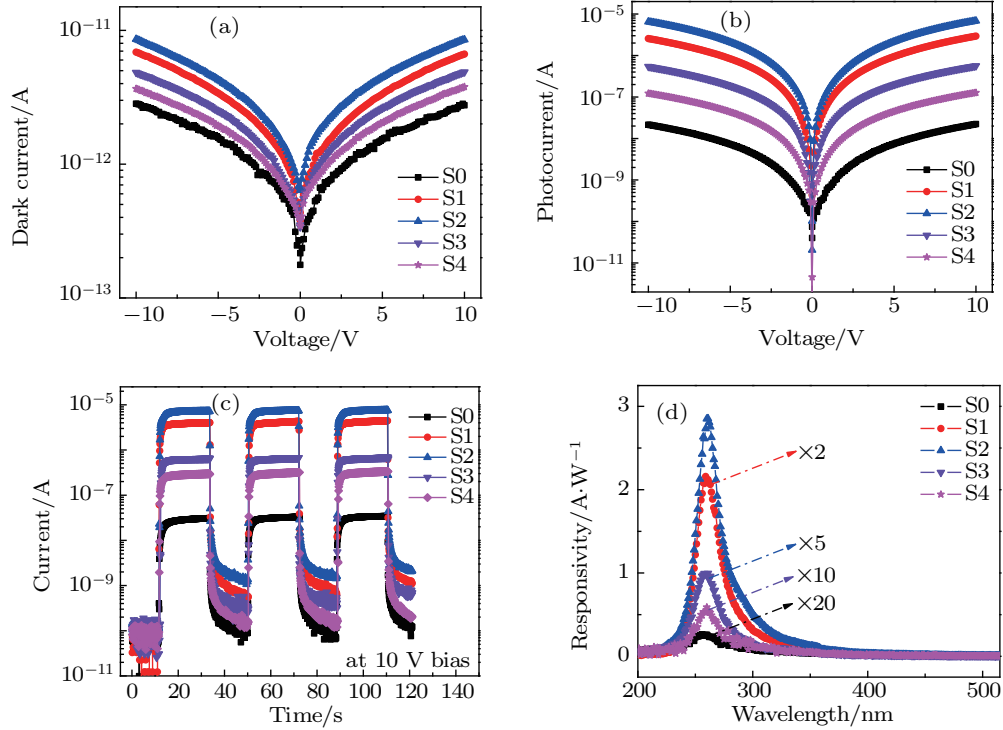


**Fig. 3.** (color online) Photoelectric properties of the PDs:  $I$ - $V$  curves (a) in the dark and (b) under 254-nm UV light illumination, (c) time-dependent photoresponse with the 254-nm UV light periodically on and off, and (d) photoresponsivity spectra of the PDs biased at 15 V.

**Table 1.** Summary of the photoelectric properties of PDs.

Samples	$I_{\text{dark}} @ 10 \text{ V/A}$	$I_{\text{photo}} @ 10 \text{ V/A}$	$I_{\text{photo}}/I_{\text{dark}}$	Responsivity/(A/W)
S0	$2.76 \times 10^{-12}$	$2.23 \times 10^{-8}$	$8.08 \times 10^3$	0.013
S1	$6.65 \times 10^{-12}$	$2.93 \times 10^{-6}$	$4.47 \times 10^5$	1.080
S2	$8.52 \times 10^{-12}$	$6.86 \times 10^{-6}$	$8.05 \times 10^5$	2.854
S3	$4.88 \times 10^{-12}$	$5.62 \times 10^{-7}$	$1.15 \times 10^5$	0.199
S4	$3.79 \times 10^{-12}$	$1.27 \times 10^{-7}$	$3.35 \times 10^4$	0.059

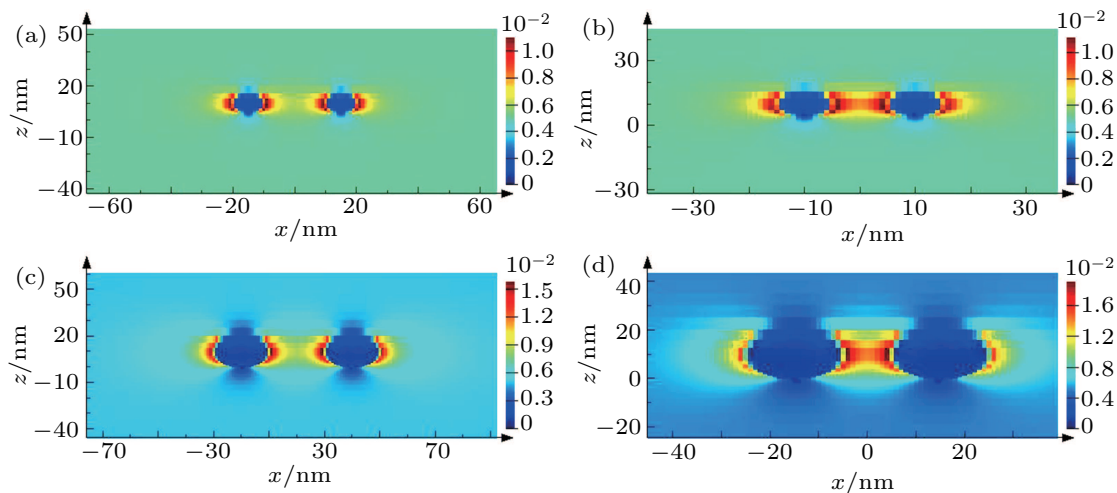


**Fig. 4.** (color online) Electric field distributions of Ga NSs in Ga<sub>2</sub>O<sub>3</sub> matrix with different diameters and gaps: (a) diameter = 10 nm and gap = 20 nm; (b) diameter = 10 nm and gap = 10 nm; (c) diameter = 20 nm and gap = 20 nm; (d) diameter = 20 nm and gap = 10 nm.

To further explore the SP performance of the Ga NS array in the surrounding Ga<sub>2</sub>O<sub>3</sub> matrix, the spatial electric field intensity distribution is simulated by the FDTD method. In order to match the results of S2, the diameters of the Ga NSs in the simulation are 10 nm and 20 nm, and the gaps between two NSs are 10 nm and 20 nm. Figures 4(a) and 4(b) show the simulated results with the diameter of 10 nm, and with the gaps of 20 nm and 10 nm, respectively. In the case of Fig. 4(a), the electric field intensity in the middle of the two NSs is slightly larger than that of the background, indicating the occurrence of a weak inter-sphere interaction. When the gap is reduced to 10 nm, the interaction between two Ga NSs becomes stronger and the area with the enhanced electric field runs through the entire range between the two NSs. Figures 4(c) and 4(d) show the typical interactions of the Ga NSs with  $d = 20$  nm and gaps of 20 nm and 10 nm, respectively. The trend of the electric field changing from Fig. 4(c) to Fig. 4(d) is the same as that for the gap of 10 nm. The electric field distribution and the inter-sphere interaction are similar to those of other metal NSs.<sup>[23,41–43]</sup> As the diameter of the metal NS increases, the electric field further strengthens and the inter-sphere interaction becomes stronger. The FDTD simulated results indicate that the local electromagnetic field around metal Ga NSs in the nanocomposite film can be greatly increased by the SP. The enhanced electric field around the metal NSs can effectively accelerate the separation of the photo-induced electron-hole pairs and thus a higher UV response can be achieved.<sup>[24,41]</sup>

#### 4. Conclusions and perspectives

A series of Ga NSs/Ga<sub>2</sub>O<sub>3</sub> nanocomposite films is acquired through post-annealing the Ga<sub>2</sub>O<sub>3</sub>/Ga/Ga<sub>2</sub>O<sub>3</sub> triple-layer films. The nanocomposite films are each composed of polycrystalline  $\beta$ -Ga<sub>2</sub>O<sub>3</sub> matrix and discrete metal Ga NSs embedded therein. The sizes of the metal Ga NSs in the nanocomposite films vary when changing the metal Ga layer thickness. The corresponding PDs demonstrate adjustable solar-blind UV photoresponse enhancement factors due to the coupling efficiency varying by tuning the morphology of Ga NSs. The maximum peak responsivity reaches 2.85 A/W at 260 nm, two orders of magnitude higher than the maximum peak responsivity of the bare Ga<sub>2</sub>O<sub>3</sub> PD. This work reveals the remarkable and tunable plasmonic coupling capability in Ga/Ga<sub>2</sub>O<sub>3</sub> systems. The results presented here are of profound significance for studying plasmonics and detecting solar-blind UV light. Meanwhile, the simple, repeatable, and cost-effective method of fabricating the high-response Ga<sub>2</sub>O<sub>3</sub> solar-blind UV PDs promises to have practical applications.

#### References

- [1] Li L, Lee P S, Yan C, Zhai T, Fang X, Liao M, Koide Y, Bando Y and Golberg D 2010 *Adv. Mater.* **22** 5145
- [2] Hou Y N, Mei Z X, Liu Z L, Zhang T C and Du X L 2011 *Appl. Phys. Lett.* **98** 103506
- [3] Liao M, Wang X, Teraji T, Koizumi S and Koide Y 2010 *Phys. Rev. B* **81** 033304

- [4] Mendoza F, Makarov V, Weiner B R and Morell G 2015 *Appl. Phys. Lett.* **107** 201605
- [5] Tut T, Yelboga T, Ulker E and Ozbay E 2008 *Appl. Phys. Lett.* **92** 103502
- [6] McClintock R, Yasan A, Minder K, Kung P and Razeghi M 2005 *Appl. Phys. Lett.* **87** 241123
- [7] Du X, Mei Z, Liu Z, Guo Y, Zhang T, Hou Y, Zhang Z, Xue Q and Kuznetsov A Y 2009 *Adv. Mater.* **21** 4625
- [8] Hou Y N, Mei Z X, Liang H L, Ye D Q, Liang S, Gu C Z and Du X L 2011 *Appl. Phys. Lett.* **98** 263501
- [9] Liang H L, Mei Z X, Zhang Q H, Gu L, Liang S, Hou Y N, Ye D Q, Gu C Z, Yu R C and Du X L 2011 *Appl. Phys. Lett.* **98** 221902
- [10] Chen X, Xu Y, Zhou D, Yang S, Ren F, Lu H, Tang K, Gu S, Zhang R, Zheng Y and Ye J 2017 *ACS Appl. Mater. Interfaces* **9** 36997
- [11] Suzuki R, Nakagomi S and Kokubun Y 2011 *Appl. Phys. Lett.* **98** 131114
- [12] Suzuki R, Nakagomi S, Kokubun Y, Arai N and Ohira S 2009 *Appl. Phys. Lett.* **94** 222102
- [13] Cui S J, Mei Z X, Zhang Y H, Liang H L and Du X L 2017 *Adv. Opt. Mater.* **5** 1700454
- [14] Singh Pratiyush A, Krishnamoorthy S, Vishnu Solanke S, Xia Z, Muralidharan R, Rajan S and Nath D N 2017 *Appl. Phys. Lett.* **110** 221107
- [15] Guo X C, Hao N H, Guo D Y, Wu Z P, An Y H, Chu X L, Li L H, Li P G, Lei M and Tang W H 2016 *J. Alloys Compd.* **660** 136
- [16] Li Y, Tokizono T, Liao M, Zhong M, Koide Y, Yamada I and Delaunay J J 2010 *Adv. Funct. Mater.* **20** 3972
- [17] Zou R, Zhang Z, Liu Q, Hu J, Sang L, Liao M and Zhang W 2014 *Small* **10** 1848
- [18] Orita M, Ohta H, Hirano M and Hosono H 2000 *Appl. Phys. Lett.* **77** 4166
- [19] Sang L, Liao M and Sumiya M 2013 *Sensors* **13** 10482
- [20] Du X, Li Z, Luan C, Wang W, Wang M, Feng X, Xiao H and Ma J 2015 *J. Mater. Sci.* **50** 3252
- [21] Barnes W L, Dereux A and Ebbesen T W 2003 *Nature* **424** 824
- [22] Schuller J A, Barnard E S, Cai W, Jun Y C, White J S and Brongersma M L 2010 *Nat. Mater.* **9** 193
- [23] Li D B, Sun X J, Jia Y P, Stockman M I, Paudel H P, Song H, Jiang H and Li Z M 2017 *Light Sci. Appl.* **6** e17038
- [24] Clavero C 2014 *Nat. Photonics* **8** 95
- [25] Chang C C, Sharma Y D, Kim Y S, Bur J A, Shenoi R V, Krishna S, Huang D and Lin S Y 2010 *Nano Lett.* **10** 1704
- [26] Tian C, Jiang D, Li B, Lin J, Zhao Y, Yuan W, Zhao J, Liang Q, Gao S, Hou J and Qin J 2014 *ACS Appl. Mater. Interfaces* **6** 2162
- [27] Li D, Sun X, Song H, Li Z, Chen Y, Jiang H and Miao G 2012 *Adv. Mater.* **24** 845
- [28] Zhang W, Xu J, Ye W, Li Y, Qi Z, Dai J, Wu Z, Chen C, Yin J, Li J, Jiang H and Fang Y 2015 *Appl. Phys. Lett.* **106** 021112
- [29] Gao H, Liu C, Jeong H E and Yang P 2012 *ACS Nano* **6** 234
- [30] Sharma B, Cardinal M F, Ross M B, Zrimsek A B, Bykov S V, Punihale D, Asher S A, Schatz G C and Van Duyne R P 2016 *Nano Lett.* **16** 7968
- [31] Losurdo M, Yi C, Suvorova A, Rubanov S, Kim T H, Giangregorio M M, Jiao W, Bergmair I, Bruno G and Brown A S 2014 *ACS Nano* **8** 3031
- [32] Catalán-Gómez S, Redondo-Cubero A, Palomares F J, Nucciarelli F and Pau J L 2017 *Nanotechnology* **28** 405705
- [33] Yang Y, Callahan J M, Kim T H, Brown A S and Everitt H O 2013 *Nano Lett.* **13** 2837
- [34] Cui S J, Mei Z X, Hou Y N, Sun M H, Chen Q S, Liang H L, Zhang Y H, Bai X D and Du X L 2018 *Sci. China-Phys. Mech. Astron.* **61** 107021
- [35] Kong W Y, Wu G A, Wang K Y, Zhang T F, Zou Y F, Wang D D and Luo L B 2016 *Adv. Mater.* **28** 10725
- [36] Zhong M, Wei Z, Meng X, Wu F and Li J 2015 *J. Alloys Compd.* **619** 572
- [37] Yu F P, Ou S L and Wu D S 2015 *Opt. Mater. Express* **5** 1240
- [38] Weng W Y, Hsueh T J, Chang S J, Huang G J and Hsueh H T 2011 *IEEE Sens. J.* **11** 999
- [39] Zhao C, Zhu Y, Su Y, Guan Z, Chen A, Ji X, Gui X, Xiang R and Tang Z 2015 *Adv. Opt. Mater.* **3** 248
- [40] Langhammer C, Schwind M, Kasemo B and Zoric I 2008 *Nano Lett.* **8** 1461
- [41] Bao G, Li D, Sun X, Jiang M, Li Z, Song H, Jiang H, Chen Y, Miao G and Zhang Z 2014 *Opt. Express* **22** 24286
- [42] Fang J, Yi Y, Ding B and Song X 2008 *Appl. Phys. Lett.* **92** 131115
- [43] Tira C, Tira D, Simon T and Astilean S 2014 *J. Mol. Struct.* **1072** 137